Journal of Geophysical Research–Planets, vol. **104**, no. **E10**, pages 24,177–24,194 (1999).

A climate database for Mars

Stephen R. Lewis, Matthew Collins,[1] and Peter L. Read

Atmospheric, Oceanic and Planetary Physics, Department of Physics, Oxford University, Oxford, England

François Forget, Frédéric Hourdin, Richard Fournier,[2] Christophe Hourdin, and Olivier Talagrand

Laboratoire de Météorologie Dynamique du CNRS, Université Paris 6, Paris

Jean-Paul Huot

European Space Research and Technology Centre, European Space Agency, Noordwijk, Netherlands

Abstract. A database of statistics which describe the climate and surface environment of Mars has been constructed directly on the basis of output from multiannual integrations of two general circulation models developed jointly at Laboratoire de Météorologie Dynamique du Centre National de la Recherche Scientifique, France, and the University of Oxford, United Kingdom, with support from the European Space Agency. The models have been developed and validated to reproduce the main features of the meteorology of Mars, as observed by past spacecraft missions. As well as the more standard statistical measures for mission design studies, the Mars Climate Database includes a novel representation of large-scale variability, using empirical eigenfunctions derived from an analysis of the full simulations, and small-scale variability using parameterizations of processes such as gravity wave propagation. The database may be used as a tool for mission planning and also provides a valuable resource for scientific studies of the Martian atmosphere. The database is described and critically compared with a representative range of currently available observations.

1. Introduction

When planning spacecraft missions to Mars, detailed information about environmental conditions on the planet is vital to reduce the chances of mission failure and to aid in the optimization of the design process. For example, aerobraking or aerocapture maneuvers require detailed knowledge of atmospheric density; when placing landers on the surface of the planet, the wind shear can be a crucial factor; and extremes of temperature in the atmosphere and on the surface must be known to prevent electronic and mechanical failures. However, direct observations of the environment of Mars are extremely sparse in both spatial and temporal coverage.

In planning previous missions to Mars, environmental statistics have been collected and summarized in the Mars Global Reference Atmosphere Model, MarsGRAM [*Justus et al.*, 1996a]. MarsGRAM uses a blend of observational data and simple physical models to produce realizations of environmental conditions. For example, temperatures are generated by fitting a series of arbitrary functions to the Mariner 9 and Viking thermal measurements, and winds are derived from this by the use of thermal wind balance. While MarsGRAM may produce reasonable fields of observable variables like surface pressure and temperature at seasons and dust loadings where observations exist, ultimately, its accuracy is limited by errors in the interpolation between sparse data and relies on the assumptions made in the physi-

[1] Now at Hadley Centre for Climate Prediction and Research, United Kingdom Meteorological Office, Bracknell, England.

[2] Now at Laboratoire d'Energie Solaire et Thermique de l'Habitat, Université Paul Sabatier, Toulouse, France.

cal formulae used to derive the unobserved variables. For example, thermal wind balance is a good approximation only in the middle to high latitudes. Winds in the equatorial regions are less well constrained by large-scale dynamical balances and can exhibit regions of strong localization, for example, western boundary currents [*Joshi et al.*, 1995]. Mars-GRAM does, however, offer the considerable advantages of being fast and easy to use.

Recently, several groups have put considerable effort into the development of general circulation models (GCMs) for Mars [e.g., *Collins et al.*, 1996a; *Haberle et al.*, 1993; *Hourdin et al.*, 1995; *Wilson and Hamilton*, 1996], and these GCMs are now at the stage where they can potentially produce realistic simulations of weather and climate. GCMs provide a self-consistent view of the environmental conditions on Mars; they are based purely on physical laws and prescribed parameters (e.g., planetary radius, rotation rate, surface roughness, etc.) without requiring ad hoc function fitting or derivation of variables using simplified balance criteria. This was recognized by the European Space Agency (ESA), who commissioned multiannual simulations of the Martian environment using a state-of-the-art GCM to produce a database of statistics, the Mars Climate Database (MCD), as a resource to aid in mission design and planning. The MCD aims to provide quick access to GCM output, sampled as specified by the user, in a way that has not been possible previously for the nonspecialist.

The development of the MCD was carried out in two main phases. First, the current state of knowledge of the Martian environment was reviewed, and two extant Mars GCMs were updated with various new parameterization schemes, validated wherever possible using observations. This task is described in more detail in a companion paper [*Forget et al.*, this issue]. Second, the GCMs were integrated over several annual cycles, using different dust distributions, and the output was collected and summarized in the form of a database. The total size of the database was limited in order to make access fast and practical on reasonably small computers. On the other hand, it was considered necessary to represent atmospheric variability on diurnal, seasonal, and interannual timescales under a range of conditions and at sufficiently high horizontal and vertical resolution to be useful. To capture the mean atmospheric diurnal and seasonal cycles, model fields were stored at 12 times of day for each season, with the Martian year split into 12 seasons. Multiannual experiments were conducted for each dust scenario, and a separate set of statistics was accumulated in each case. These statistics give the climatological mean and variance for each field of interest, but it is also desirable for some purposes to be able to produce a realistic ensemble of individual profiles representing plausible instantaneous atmospheric states. This is achieved in the MCD by the application of statistical-dynamical models of the large-scale, day-to-day GCM variability within each season, for example, owing to weather systems, and the small scale motions which are often parameterized in a GCM, for example, vertically propagating gravity waves.

Table 1. Mars Climate Database Variables

Mean and Standard Deviation	Units
Atmospheric temperature	K
Zonal (E-W) wind	$\mathrm{m\,s^{-1}}$
Meridional (N-S) wind	$\mathrm{m\,s^{-1}}$
Atmospheric density	$\mathrm{kg\,m^{-3}}$
Turbulent kinetic energy	$\mathrm{m^2\,s^{-2}}$
Surface pressure	Pa
Surface temperature	K
Surface emissivity	none
CO_2 ice cover	$\mathrm{kg\,m^{-2}}$

Of course, mission design engineers are not the only potential users of such a climatological database, containing as it does a fully self-consistent collection of statistics from an ensemble of multiannual simulations using a well verified model. Climatological statistics are also of great value and interest for members of the scientific community concerned with developing an understanding of the Martian climate and meteorology on timescales of hours to years. As will be discussed below, because of its logical organization and easy accessibility via commonly available meteorological analysis and visualization packages, the database described herein is well suited to a wide range of scientific studies of the Martian atmosphere and near-surface environment. Its structure and formulation may therefore serve as a valuable model for other groups to emulate, both as a means of summarizing complex data sets arising from long-term GCM simulations and as a vehicle for detailed quantitative intercomparisons of simulated climatologies between different models.

This paper describes the structure of the MCD in detail and presents a critical comparison between output from the database and currently available spacecraft observations of Mars. The appendix briefly describes the methods by which the MCD may be accessed.

2. Database Structure

2.1. Variables Stored

The variables stored in the database are shown in Table 1. The main model dynamical prognostic variables, atmospheric temperature, zonal wind, meridional wind, and surface pressure are stored, as well as atmospheric density, which is important in spacecraft mission design. The boundary layer eddy kinetic energy, which is a prognostic variable in the boundary layer scheme [*Forget et al.*, this issue], is stored and can give some indication of turbulence intensity. Also stored are various surface fields, surface temperature, CO_2 ice cover, and surface emissivity, which vary when CO_2 snow falls [*Forget et al.*, 1998]. The database also includes time invariant fields of surface topographic height and subgrid-scale topographic standard deviation.

Table 2. Mars Climate Database Seasons

Season	L_S	Day
1	0°–30°	0–61
2	30°–60°	61–127
3	60°–90°	127–193
4	90°–120°	193–258
5	120°–150°	258–318
6	150°–180°	318–372
7	180°–210°	372–422
8	210°–240°	422–468
9	240°–270°	468–515
10	270°–300°	515–562
11	300°–330°	562–613
12	330°–360°	613–669

2.2. Temporal Structure

It would be desirable to have a complete record of the model history for all the simulations performed, stored at every model grid point and with as high a temporal resolution as possible. However, simply storing the model history for even one Martian year results in a data set that is much too large to handle on a day-to-day basis, even using the most up to date workstations and fast storage media. In order to reduce the mass storage requirement some temporal averaging of the model output was performed. Reducing the spatial resolution of the model output was ruled out because details in the Martian topography become smeared out at low horizontal resolution and large gradients in variables, such as wind speed and direction, must be resolved, for example, for lander design. Some novel techniques were developed for simulating the variability destroyed during the temporal averaging process (see section 4.1).

In order to resolve the large annual cycle observed in many variables such as surface pressure (see Figure 7a) we chose to split the Martian year into 12 seasons of equal length in areocentric longitude, L_S, given in Table 2. In Table 2, and elsewhere throughout this paper, a "day" is taken to mean a Martian solar day (about 88,775 s), and an "hour" is taken to mean 1/24th of a solar day. Within each season we store mean values of each variable at 12 universal times in order to resolve the large Martian diurnal tide. Also, the diurnally averaged standard deviation of every variable is stored for each season in order to represent all the variability not associated with the mean diurnal cycle. Such variability is due both to the passage of weather systems and to any intraseasonal trend, for example, pressure variations resulting from the CO_2 condensation cycle.

2.3. Horizontal Structure

Variables in the database are written on a horizontal grid of 96 longitude points by 48 latitude points equally spaced by $3.75°$ in each direction, a grid spacing of about 225 km at the equator. This grid resolution is comparable to that in models employed in the terrestrial climate modeling community [e.g., *Gates*, 1992].

One of the major uncertainties in the Mars GCMs is the prescription of the surface topography. The United States Geological Survey's Digital Topographic Map (DTM) of Mars [*NASA*, 1993] was chosen for the main set of model runs that were used to compile the MCD because of its complete global coverage and small-scale detail, the latter of which is an important input parameter for the gravity wave and form drag scheme [*Collins et al.*, 1997], though the possibility of large-scale biases in the mean topography is a concern. Another commonly used topographic map, which is substantially different from the DTM, is known as the Consortium data set [*Wu*, 1978] and was derived from Mariner 9 radio occultations and gravity field measurements [*Christensen*, 1975; *Lindal et al.*, 1979]. The sensitivity of the model climate to the differences between the DTM and Consortium data was tested by comparing climate statistics from model integrations with each topography. For many applications, such as deriving vertical atmospheric density and temperature profiles, the MCD results were found to be robust to the differences between the topographic data sets; agreement was much better than the level of intrinsic model variability. However, some other aspects, such as low-level wind direction, are sensitive to topography, and it will clearly be desirable to update the MCD once definitive results from the Mars

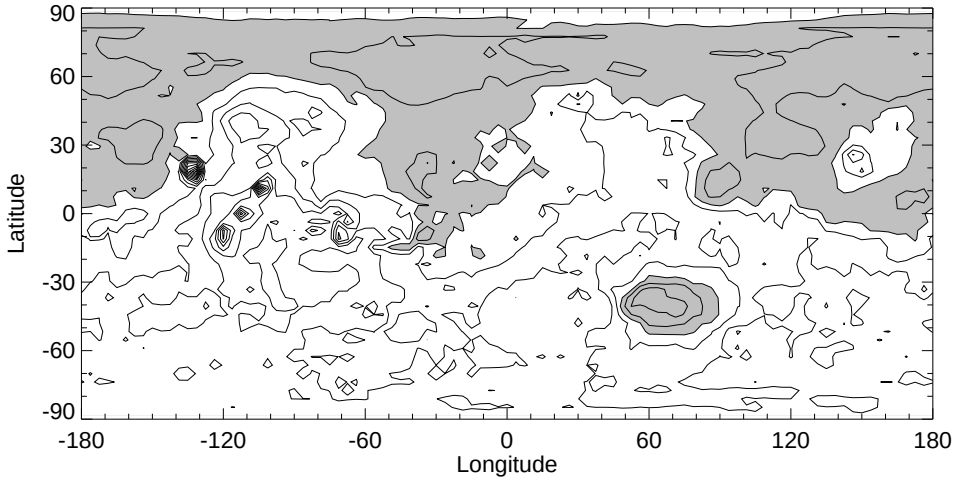

Figure 1. The Digital Topographic Map smoothed to database resolution on a horizontal grid of 96 longitude by 48 latitude points. Regions below the reference geoid are shaded; the contour interval is 2 km.

Orbiter Laser Altimeter (MOLA) experiment [*Smith et al.*, 1998] aboard the Mars Global Surveyor spacecraft become available. The DTM topography smoothed for the GCMs to be run at the database resolution is shown in Figure 1. The spatial resolution is sufficiently fine to pick out prominent features such as the Tharsis volcanoes and Olympus Mons, as well as to capture larger features like the Hellas basin.

2.4. Vertical Structure

The database vertical coordinate is based on the terrain-following σ coordinate, in keeping with the GCMs, and defined as

$$\sigma = p/p_* \tag{1}$$

where p is the atmospheric pressure and p_* is the surface pressure. Thus $\sigma = 1$ at the surface, $\sigma = 0$ at infinite height, and the σ levels follow the database topography. This overcomes many problems in the definition of the database grid as, for example, atmospheric levels may intersect the surface when a pressure or geometric height coordinate is used. The sigma levels are arranged as in Table 3, which also gives approximate altitudes above the local surface on the basis of the assumption of a constant atmospheric scale height of 10 km. When using the MCD interface software, σ is converted to either pressure or geometric height using the surface pressure and integration of the hydrostatic equation using the local temperature profile. The σ level spacing is stretched in order to have fine resolution in the boundary layer near the surface to represent large gradients, for example, strong temperature inversions which form at night. At upper levels the vertical resolution tends to about half a scale height until the upper sponge layers are reached, which are more widely spaced. Above the model top, the variables may be extrapolated in straightforward ways, or the model database may be merged into a simple thermosphere model, such as that supplied with MarsGRAM [*Justus et al.*, 1996b], with input parameters determined from the MCD predictions in the lower atmosphere.

3. Dust Distribution Scenarios

The major factor which governs the interannual variability in the Martian atmosphere is the amount and distribution of suspended dust. Some years may have low or moderate dust loading throughout the year, while others may have regional or global dust storms which engulf the planet for several tens of days, especially during northern winter [e.g., *Zurek et al.*, 1992]. Multiannual experiments were conducted in order to provide statistics for all 12 seasons from several different years. In practice, very little interannual variability was found in the mean data under each prescribed dust distribution scenario, and data from the first two model years (initialized from a model which had been previously spun up for many years to establish the soil temperature and CO_2 ice cycle) were averaged to form the MCD.

Multiannual model integrations were carried out for the database under two main dust scenarios: (1) seasonally varying dust, modeled on that observed during the Viking Lander years [*Zurek and Martin*, 1993] but with the large dust storms removed and (2) low, uniform dust, appropriate to

Table 3. Mars Climate Database σ Levels

Level	σ	Altitude
1	0.999500	5 m
2	0.998098	19 m
3	0.995562	44 m
4	0.990977	91 m
5	0.982737	174 m
6	0.968097	324 m
7	0.942591	591 m
8	0.899629	1.1 km
9	0.831173	1.8 km
10	0.731006	3.2 km
11	0.600911	5.1 km
12	0.455263	7.9 km
13	0.316690	11.5 km
14	0.203944	15.9 km
15	0.123568	20.9 km
16	0.071666	26.4 km
17	0.040323	32.1 km
18	0.022181	38.1 km
19	0.011955	44.3 km
20	0.006290	50.7 km
21	0.003199	57.4 km
22	0.001542	64.7 km
23	0.000678	73.0 km
24	0.000250	83.0 km
25	0.000056	97.8 km

a clearer, colder Mars. The first, Viking, scenario results in a reasonable fit between model results and both Viking and subsequent Pathfinder observations, as described below. Microwave observations of Martian atmospheric temperature [*Clancy et al.*, 1996] have indicated colder temperatures than those observed by the Viking infrared thermal mapper (IRTM), although there is now evidence that the IRTM observations suffer from a warm bias [*Wilson and Richardson*, 1999] and so the measurements may in fact be consistent. Phobos 2 observations also indicate that less dusty conditions than those indicated by the Viking Lander data are a possibility [*Chassefiere et al.*, 1995]. The inclusion of data from both the Viking dust scenario and the low-dust scenario in the MCD is intended to reflect the current uncertainty in the appropriate background dust loading of the Martian atmosphere and to provide warm and cold extremes (in the absence of major dust storms) for studies which require a plausible range of conditions.

In addition to the full annual data sets, scenarios were conducted for several seasons with much higher dust loadings, $\tau = 2$ and $\tau = 5$, appropriate to dust storm conditions. There is good evidence [*Zurek et al.*, 1992] that the dust optical depth may exceed $\tau = 2$ during dust storms and reach $\tau = 5$ or greater; hence the inclusion of these scenarios in the database.

The dust optical properties used in the GCM simulations which form the MCD illustrated here are dicussed further by *Forget et al.* [this issue] with the dust single scattering albedo based on *Clancy and Lee* [1991]. Details of the dust distribution scenarios are given below.

3.1. Viking Scenario

The total dust optical depth for the Viking scenario was specified as a function of time to model the Viking observations [*Zurek and Martin*, 1993] with peaks representing dust storms removed (illustrated in Figure 2):

$$\tau = 0.7 + 0.3\cos(L_S + 80^\circ) \tag{2}$$

where τ is the optical depth at a reference pressure $p_0 = 700\,\mathrm{Pa}$ and L_S is the areocentric longitude of Mars. The optical depth was taken to be uniform in the horizontal for the baseline integrations; spatial variations have been observed but have no simple dependence on position [*Martin and Richardson*, 1993]. However, the top of the dust layer was specified as a function of both time and latitude, in a way intended to represent the results of limb observations from both Mariner 9 [*Anderson and Leovy*, 1978] and Viking [*Jaquin et al.*, 1986]:

$$z_{\max}(L_S, \phi) = \left(60 + 18\sin(L_S - 160^\circ) - 22\sin^2\phi\right)\ \mathrm{km} \tag{3}$$

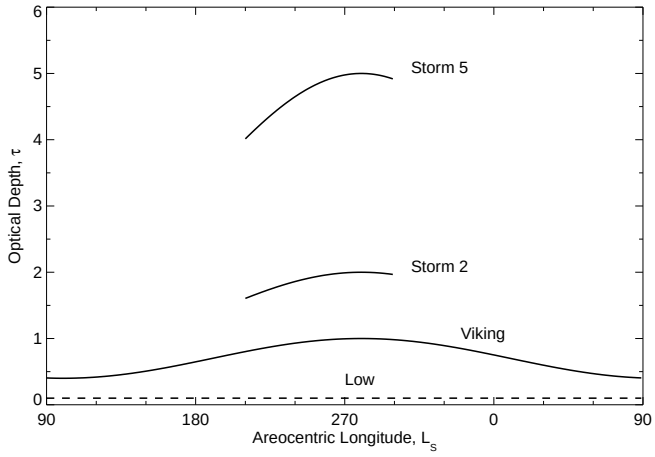

Figure 2. Dust optical depth at 700 Pa as a function of time of year. The areocentric longitude L_S is defined such that $L_s = 0°$ is the Northern Hemisphere vernal equinox. Curves are plotted for each dust scenario described in the text.

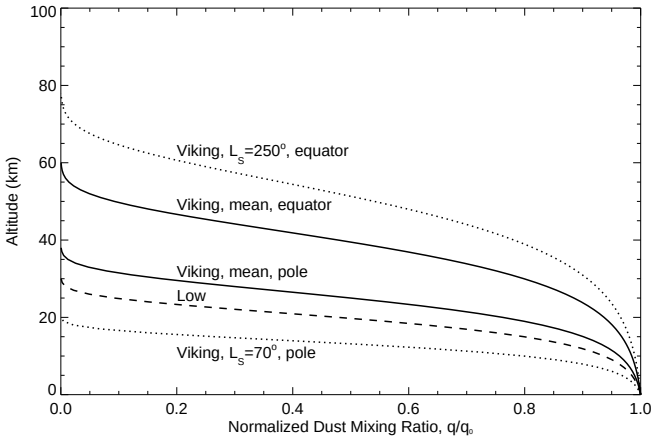

Figure 3. The variation of dust mixing ratio with height, normalized by the value at 700 Pa. Profiles are shown for the Viking dust scenario, with annual means at the equator and pole and the extreme highest and lowest dust layers, and for the low-dust scenario.

where ϕ is the latitude. The dust layer top $z_{\max}$, which varies between 78 km at the equator during the dusty seasons and 20 km at the pole during the clear seasons, is a parameter in the equation which was used to describe the vertical variation of dust mixing ratio q,

$$q = q_0 \exp\left\{0.007\left[1 - (p_0/p)^{(70\ \mathrm{km}/z_{\max})}\right]\right\} \qquad (4)$$

for pressure $p \leq p_0$, with $q = q_0$ for $p > p_0$, as described by *Forget et al.* [this issue]. Profiles of the assumed dust mixing ratio are illustrated in Figure 3.

3.2. Low-Dust Scenario

The low-dust scenario was conducted with a dust distribution which was chosen to be invariant in latitude, longitude, and time, with an optical depth of $\tau = 0.1$ and the vertical cutoff at at $z_{\max} = 30$ km altitude. This scenario was designed to provide a cold extreme for the database.

3.3. Dust Storm, $\tau = 2$

A moderate, global dust storm scenario was conducted using parameters similar to those of the Viking scenario, with the vertical cutoff for the dust modeled as (3) but with double the dust optical depth given by equation (2), which then peaks at $\tau = 2$. Statistics were stored only for the northern winter seasons, when dust storms are most likely to occur; seasons 8–10 correspond to L_S =210°–300°.

3.4. Dust Storm, $\tau = 5$

This represents a heavy, global dust storm, conducted as the $\tau = 2$ storm scenario but with the Viking scenario dust optical depth multiplied by five, to peak at $\tau = 5$. As with the moderate dust storm, statistics were stored only for seasons 8–10, L_S =210°–300°.

4. Variability

4.1. Large-Scale Variability Model

As described in section 2.1, mean fields in the MCD are stored once a season, a season being typically 50–70 days long. Although the component of the variability which is due to the diurnal cycle is largely captured by storing the seasonally averaged fields at 12 times of day, there may still be significant variation about the mean owing to, for example, motions of baroclinic weather systems. This large-scale, or model-resolved, variability can be significant when compared to the time mean and may be crucial in mission planning. Figure 4 shows a selection of vertical profiles of temperature and normalized density taken once a day during one season at a midlatitude point in the winter hemisphere in the

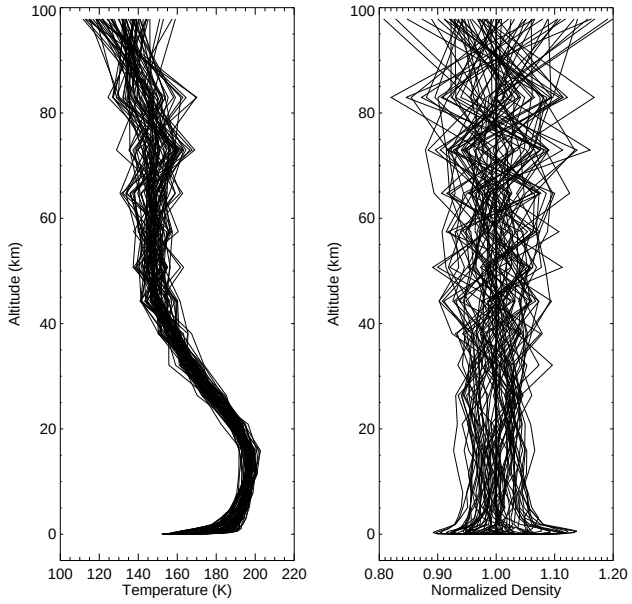

Figure 4. Profiles of temperature and normalized density from a single point (42.5°S, 0°W) in the general circulation model sampled once a day at midnight throughout database season 4.

GCM. The density has been normalized by its mean profile to show the variation as a function of altitude more clearly. A winter season was chosen since this displays the largest day-to-day variations with the passage of weather systems. It is necessary to simulate these profiles in some way in order to capture the model variability destroyed during the temporal averaging of the model history. This is particularly important if profiles are required with realistic vertical gradients, for example. While the climatological mean and variance fields could be used to give estimates of a variable at one point, they do not contain information about correlations between the variability at different locations and between different variables. The large-scale variability model is an attempt to reconstruct this information from the GCM results.

Large-scale variability in the database is represented using a novel approach based on a technique that is widely used in meteorological data analysis, as well as in other subject areas, namely, empirical orthogonal function (EOF) analysis [e.g., *Mo and Ghil*, 1987; *North*, 1984]. This involves finding the eigenvalues and eigenvectors of the covariance matrix of a set of data vectors. The eigenvectors, or EOFs, form a linear basis for the data such that those with the largest eigenvalues account for the most variance. The "variance compression" nature of the EOFs means that one can reconstruct the main characteristics of the original data from a limited set of EOFs and corresponding time coefficients, sometimes called principal components (PCs). In the special case of data contaminated with uncorrelated noise, the EOFs separate the "signal" from the "noise."

If $\overline{\mathbf{D}}$ is a vector representing the database mean profile of a meteorological variable, we form a new profile $\mathbf{D}$ by adding a series of vectors to the mean profile:

$$\mathbf{D} = \overline{\mathbf{D}} + \sum_{i=1}^{N} p_i \mathbf{e}_i \tag{5}$$

where the vectors $\mathbf{e}_i$ are the EOFs of the covariance matrix computed from profiles extracted once a day from the full GCM history and the scalars p_i are the principal components, which can be thought of as the projection of the EOFs onto the original model history profiles. N is the truncation, which must be small enough to limit storage requirements while being large enough to capture a significant portion of the profile variance.

Commonly in meteorology, EOFs are computed for single variables only. For the present application, however, it is desirable to compute multivariate EOFs of the main atmospheric variables: surface pressure, atmospheric temperature, zonal and meridional wind, and density. There is significant cross correlation between dynamical variables because the processes which generate such variability are generally large-scale features, such as baroclinic waves with wavenumbers in the longitudinal direction of typically one, two, or three. To form multivariate EOFs, we first renormalize individual variables to have unit variance so that all quantities have equal weight in the analysis. We also compute the EOFs on a low-resolution, $20^\circ \times 20^\circ$ grid. This is justified as, in general, the processes we mean to represent have a large spatial scale. This assumption has been tested by calculating EOFs at the full database resolution and comparing the results.

In practice, the series in (5) is truncated to 6 EOFs, which, on average, captures about 90% of the total variance. This is enough to represent the gross characteristics of the variability while limiting the storage required to manageable levels. The time coefficients or PCs, p_i, are modeled using a second-order polynomial fit in time, to capture any seasonal trend, plus a scaled random element, to capture transient oscillatory phenomena. The algorithm is described in some more detail by *Collins et al.* [1996b]. An example of some simulated profiles is shown in Figure 5; these are statistically similar to the original profiles shown in Figure 4, except for the slightly lower variance, mainly at the grid length scale, in Figure 5, which is due to the truncation of the EOF series.

Future releases of the MCD will employ an EOF model with two spatial dimensions, allowing for both realistic ver-

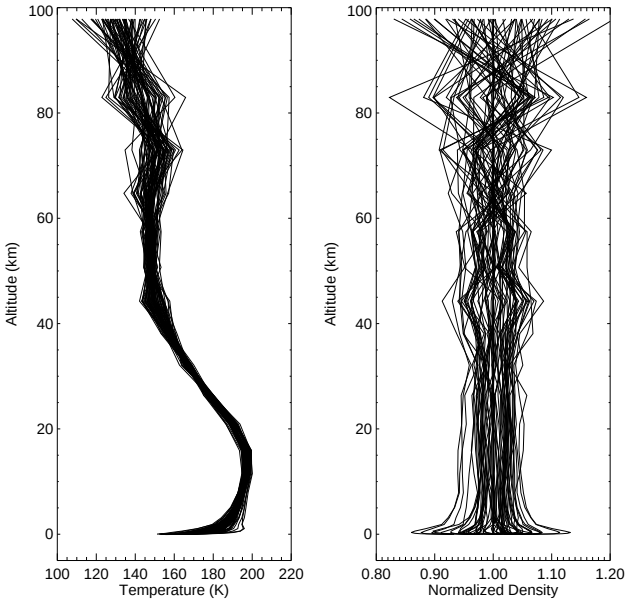

Figure 5. Profiles simulated using the Mars Climate Database (MCD) empirical orthogonal function model, at the same point and times as those shown in Figure 4.

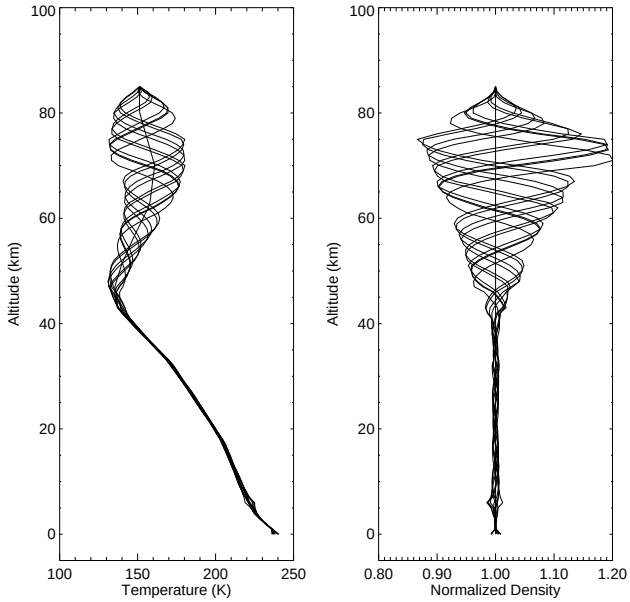

Figure 6. A series of 10 perturbations generated by the small-scale variability model added to mean profiles of temperature and density from the MCD; these correspond to the Viking Lander 1 entry location and time when gravity wave activity is predicted to be significant by the model.

tical and horizontal correlations in the large-scale variability.

4.2. Small-Scale Variability Model

Despite increases in computational power, in general, it is not possible to run GCMs at sufficiently high resolution to simulate accurately the effects of vertically propagating inertia-gravity waves. These small-scale waves can feed back on the large-scale circulation of the atmosphere [e.g., *Palmer et al.*, 1986]. Therefore we have introduced a parameterization of these effects in the Mars GCM used to generate the database [*Collins et al.*, 1997; *Forget et al.*, this issue]. There is a corresponding need to simulate small-scale gravity wave behavior in the MCD to generate realistic profiles. For this we have developed a model which simulates perturbations of density, temperature, and wind due to the upward propagation of small-scale gravity waves. The model is based on the parameterization scheme used in the GCM.

The surface stress exerted by a vertically propagating, stationary gravity wave can be written

$$\tau_0 \;=\; \kappa\rho_0 N_0 |\mathbf{v_0}| \sigma_0 \tag{6}$$

where κ is a characteristic gravity wave horizontal wave number, ρ_0 is the surface density, N_0 is the surface Brunt-Väisälä frequency, $\mathbf{v_0}$ is the surface wind vector, and σ_0 is a measure of the model subgrid-scale orographic variance.

Following *Palmer et al.* [1986], this surface stress can be related to the gravity wave vertical isentropic displacement δh by

$$\tau_0 \;=\; \kappa\rho_0 N_0 |\mathbf{v_0}| \delta h^2. \tag{7}$$

We then assume that the stress τ above the surface is equal to that at the surface. This leads to an expression for δh at height z:

$$\delta h \;=\; \sqrt{\frac{\rho_0 N_0 |\mathbf{v_0}| \sigma_0}{\rho N |\mathbf{v}|}} \tag{8}$$

where ρ, N, and $\mathbf{v}$ are the density, Brunt-Väisälä frequency, and wind vector at height z, respectively.

The gravity wave perturbation to a meteorological variable is calculated by considering vertical displacements of the form

$$\delta z = \delta h \sin\left(\frac{2\pi z}{\lambda} + \phi_0\right) \tag{9}$$

where λ is a characteristic vertical wavelength for the gravity wave and ϕ_0 is a randomly generated surface phase angle. Perturbations to temperature, density, and wind at height z are then found by using the value at $z+\delta z$ on the background profile, with the perturbations to temperature and density

calculated on the assumption of adiabatic motion to the valid height. A value can be chosen for λ to provide a reasonable comparison with the observed Viking entry temperature profiles above 50 km (Figures 8a and 8b); we take $\lambda = 16$ km, though, in practice, a spectrum of gravity waves would be more realistic if there were sufficient data to calibrate such a model. An example of several small-scale perturbations is shown in Figure 6. Deficiencies of the current small-scale variability model, apparent in this diagram, are that the gravity wave perturbations are monochromatic, and, unlike the full GCM parameterization, the waves cannot break below the model top, although this aspect should be improved in the future. As can be seen in Figure 6, it is possible for gravity waves to result in large perturbations to an individual profile, especially at high altitudes.

5. Validation of the Mars Climate Database

This section describes a comparison of previous spacecraft observations of Mars with results predicted at similar locations and times in the MCD, in effect, a validation of the GCMs themselves which were used to generate the database. It should be remembered that the MCD has been compiled with temporal averaging, and thus the few individual observations could not be expected to match the climatology, even if the true dust conditions, which are in general poorly known, matched one of the MCD scenarios exactly. The variability models provided with the MCD do allow an ensemble of realizations consistent with climatology to be produced. The extent to which these differ indicates the degree of confidence which may be placed in any one prediction. Comparisons are made with observations of surface pressure, temperature, wind, and polar ice caps. Validation against the recent Mars Pathfinder observations is dealt with in a separate section since these observations permit a validation of the MCD diurnal cycle, in particular, in several variables. Mars Pathfinder provides the first real test of the MCD since the latter was designed and compiled from model runs conducted before these data became available.

5.1. Surface Pressure

During the Viking mission, two landers collected meteorological observations for several Martian years from the northern hemisphere of the planet (Viking lander 1 was situated at 22°N, 48°W; Viking lander 2 was situated at 48°N, 226°W). Figure 7a shows the Viking 1 and 2 daily averaged surface pressure observations taken from the first Martian year of the mission. The seasonal cycle is due largely to the condensation and sublimation of CO_2, although there is an important dynamical component [*Hourdin et al.*, 1993], while the high-frequency oscillations are due to weather systems passing over the landers [*Barnes*, 1980, 1981; *Collins et al.*, 1996a]. Figure 7b shows the MCD Viking dust scenario daily-averaged pressure from the Viking sites. An estimate of the variability due to weather systems, with the seasonal trend component of the MCD variance removed, is also shown. The variance is large in the winter season, in good agreement with the observations, as is the overall shape of the pressure curves. The annual-mean pressure at each site and the pressure difference between the two sites are, however, sensitive to the choice of topographic data set and to the database resolution.

Also shown is the mean pressure from the $\tau = 5$ dust storm scenario at the same time of year as the dust storm seen in Figure 7a, confirming that pressures are higher and the variability is somewhat lower at these points under dust storm conditions, consistent with the observations. It should be noted that the dust storm scenario implies a globally uniform storm, which is not necessarily the case in reality, and the actual optical depth may not have been as high as $\tau = 5$ throughout the storm observed by the Viking landers [*Zurek and Martin*, 1993]. Hence some features, for example, the size of the pressure increase at the Viking Lander 1 site, will not necessarily match observations.

5.2. Temperature

Temperature observations from the Martian atmosphere have been obtained from both direct measurements and from a variety of remote-sensing measurements from the Earth and from orbiting spacecraft.

Figures 8a and 8b show temperature measurements taken during the entry phases of the Viking landers [*Seiff and Kirk*, 1977] compared with MCD simulations of these profiles. The MCD profiles were generated using the access software (see the appendix) and are bilinear interpolates to the locations of the Viking entry sites (22°N, 48°W and 48°N, 226°W) at the closest local time of day at which means are stored in the database to the true entry times; the actual entry times were 1613 and 0906 LT and the MCD local solar times for the seasonal composites were 1648 and 0856 LT for Viking 1 and 2, respectively. Both MCD profiles were formed from means taken over database season 4 ($L_S = 90°$–$120°$), a period when the dust optical depth is close to its minimum value, $\tau = 0.4$, in the Viking dust scenario (see equation (2)); the actual areocentric longitudes at which Viking 1 and 2 arrived were $L_S = 96°$and $L_S = 117°$respectively. Figures 8a and 8b show the mean temperature from the Viking dust scenario together with an example profile which makes use of the large- and small-scale variability models with an arbitrary random number seed (9999 in both cases). The small-scale variability is representative of vertically propagating gravity waves, ap-

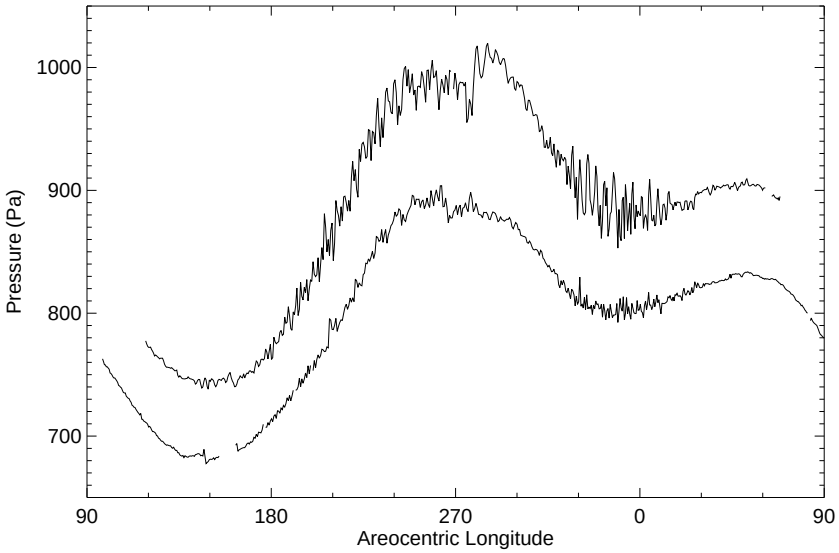

Figure 7a. Observed Viking 1 (bottom curve) and 2 (top curve) surface pressure for the first Martian year of observations, filtered to remove the diurnal tide. The high-frequency oscillations are caused by weather systems passing over the landers. The jump in pressure, and modulation in the amplitude of the weather signal, close to $L_S = 280°$ was caused by a dust storm. (Data from the Atmospheres Node of the Planetary Data System.)

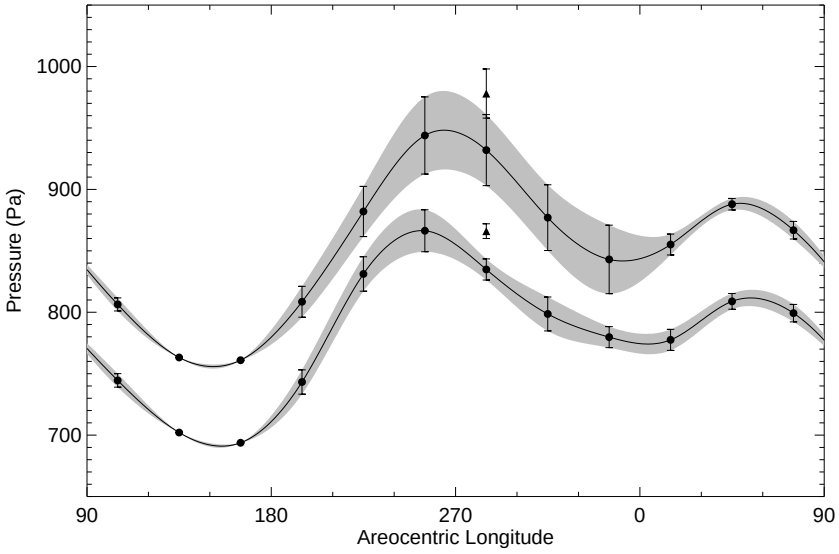

Figure 7b. Pressure at the Viking 1 (bottom curve) and 2 (top curve) sites for 1 year of the MCD Viking dust scenario. The solid circles show the diurnally averaged, seasonal values at intervals of $30° L_S$, and the smooth curve is a cubic spline fit. The error bars and shaded region indicate the nondiurnal variability (2σ) of the surface pressure with the seasonal trend component removed from the total variance. The triangles and error bars at $L_S = 285°$ show the pressure and nondiurnal variance at this time in the $\tau = 5$ dust storm scenario.

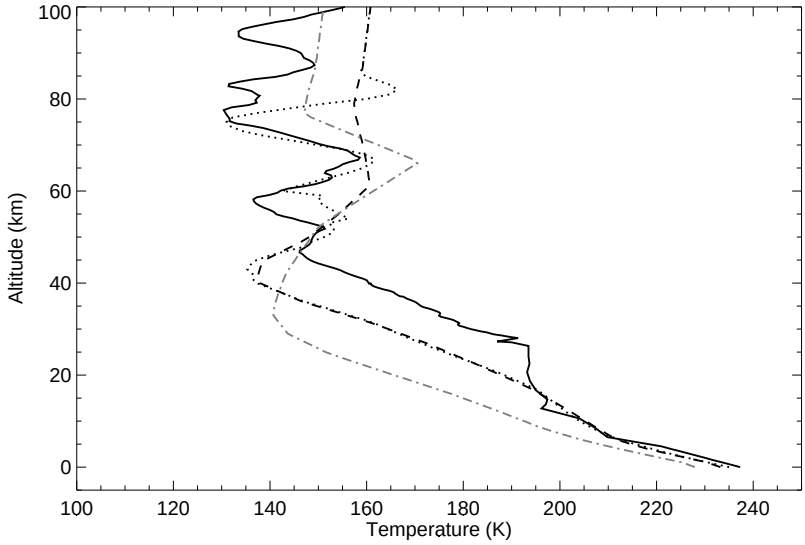

Figure 8a. The Viking Lander 1 entry temperature profile (solid line), shown with the MCD climatological mean (dashed line) from the Viking dust scenario, season 4, and one application of the MCD large- and small-scale variability models (dotted line). The gray, dot-dashed line shows the low-dust scenario mean profile for the same location and time for comparison. The altitude axis shows the height above the local surface. (Viking data provided by A. Seiff and J. R. Murphy, 1998.)

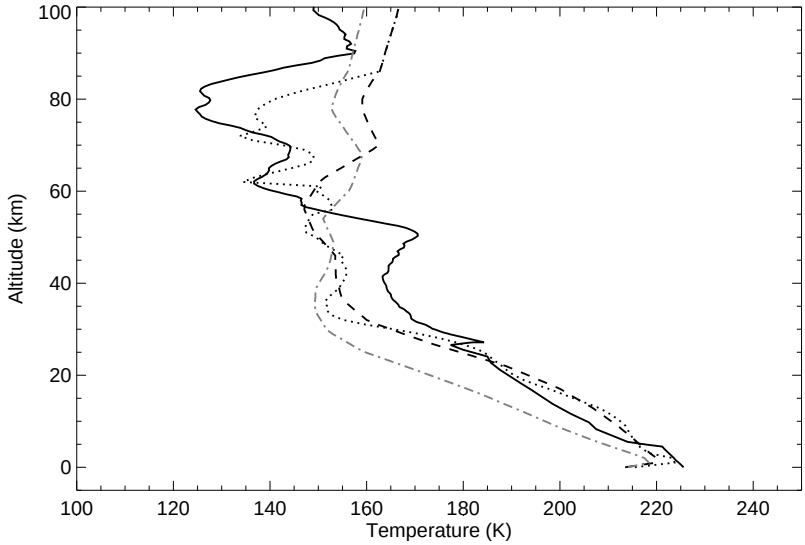

Figure 8b. The Viking Lander 2 entry temperature profile (solid line), shown with MCD climatologies and variability, labeled as in Figure 8a. (Viking data provided by A. Seiff and J. R. Murphy, 1998.)

plied with random phase, and is most important at higher altitudes where the observations also seem to indicate wave-like behavior, though it is not clear to what extent this is due to gravity waves or thermal tides in the observations. Mean temperature profiles from the low-dust scenario at the same season and time of day are also shown for comparison. These provide a cold lower bound on the temperature estimate for the lower atmosphere.

The agreement with the observations appears generally reasonable and is particularly good in the lower atmosphere from the surface up to about 20–30 km. There is some indication that the MCD is underestimating temperatures in the 20–50 km region compared to the individual observations. This might be a result of the current simple specification of dust distribution; variations in the dust distribution globally or locally could account for the temperatures observed. Were more dust to be mixed to higher levels, this would increase model temperatures in this region. Above about 80 km altitude, nonlocal thermodynamic equilibrium effects begin to become significant [*Lopez-Valverde and Lopez-Puertas*, 1994]; these are currently treated only simply in the model radiation schemes, but an improved treatment to extend the upper limit of the GCMs is planned.

The majority of temperature observations of the Martian atmosphere come from remote sensing of the atmosphere by instruments mounted on orbiting spacecraft. Figures 9a, 9b, and 9c show a comparison of the MCD low-dust and Viking dust scenario temperatures, zonally averaged for the appropriate season, with the temperatures shown by *Leovy* [1982] from the Mariner 9 infrared interferometer spectrometer (IRIS) instrument at $L_S = 43°$–$54°$. There appears to be a good agreement, especially considering that a zonal average is being compared with observations which may not sample the atmosphere in the same way. The observed temperatures are closer to the Viking dust scenario, particularly above 10 km altitude, where the low-dust scenario is too cold. This suggests that insufficient dust is mixed in this region of the atmosphere in the low-dust scenario compared to the Martian atmosphere at the time of the IRIS observations, although temperatures near the surface appear reasonable. In the lower atmosphere, below 10 km, the Viking scenario is slightly warmer than observations in northern mid-latitudes, perhaps suggesting that the total dust loading is too high in this case. The different annual dust scenarios within the MCD currently allow a realistic range of possibilities to be considered, from the relatively warm Viking scenario to the colder, low-dust scenario, and these effectively bracket the range of observed temperatures.

5.3. Wind

Direct observations of winds on Mars are extremely rare [*Zurek et al.*, 1992]. However, winds have been inferred from a variety of secondary effects, such as streak features on the Martian surface [*Thomas et al.*, 1984]. These observations suffer from problems of incomplete global coverage and uncertainties in exactly how and when the features were formed but have previously been used as a basis for a comparison with the Ames Mars GCM [*Greeley et al.*, 1993]. Figure 10a shows a set of wind directions inferred from wind streak data [*Magalhães*, 1987]; these can be compared with low-level winds from the MCD, shown in Figure 10b, for the period $L_s = 270°$–$300°$ corresponding to the approximate time at which the streaks might have formed and under medium, $\tau = 2$, dust storm conditions, since the streaks are thought to have formed during the decay phase of a global dust storm. The mean wind direction at this level, shown on the right of Figure 10b, is actually rather insensitive to dust loading, and similar patterns are obtained from the Viking and $\tau = 5$ dust storm scenarios. Although there are considerable uncertainties in the appropriate dust loading, range of times to average over, and heights at which to sample the winds, Figures 10a and 10b do show strong similarities. In particular, both zonally averaged diagrams show evidence of predominant westerlies at high northern latitudes, a region of northeasterlies north of the equator with rotation back to northwesterlies in the southern midlatitudes. This pattern in the subtropics is consistent with a single, cross-equatorial cell in the mean meridional circulation [*Magalhães*, 1987]. There are also similarities in the MCD wind and observed streak directions in the longitude–latitude maps in several regions where there are observations. For example, there are coherent regions of northerly, cross-equatorial flow near 50°W and 120°E in Figures 10a and 10b, consistent with western boundary current at the edge of the Tharsis and Syrtis Major ridges [*Joshi et al.*, 1995]. Difficulties in the interpretation of the streak data make a strict comparison impossible, but we conclude that the database winds appear generally consistent with the observations.

5.4. Polar Caps

Figure 11 shows the time-mean equivalent latitudes for the edges of the polar caps of carbon dioxide ice for the four scenarios from the MCD. The equivalent latitude is that which would be reached by a perfectly symmetrical cap occupying the same area as the total area of ice coverage in that hemisphere. Also shown are actual observations of the edges of the Martian ice caps for comparison. The agreement appears good, indicating that the climatological surface temperature, and hence conditions for CO_2 ice formation and

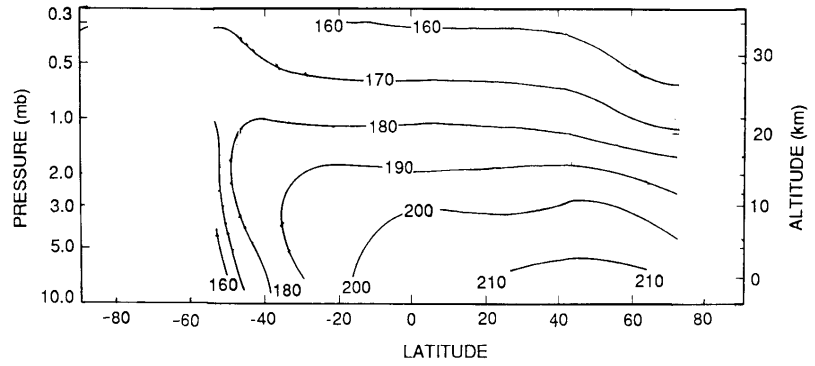

Figure 9a. The temperature (K) structure observed by the infrared interferometer spectrometer (IRIS) instrument on Mariner 9 in 1972 during northern spring ($L_S = 43°–54°$). (Adapted from *Leovy* [1982] (with permission from Elsevier Science) from data provided by B. Conrath, 1982.)

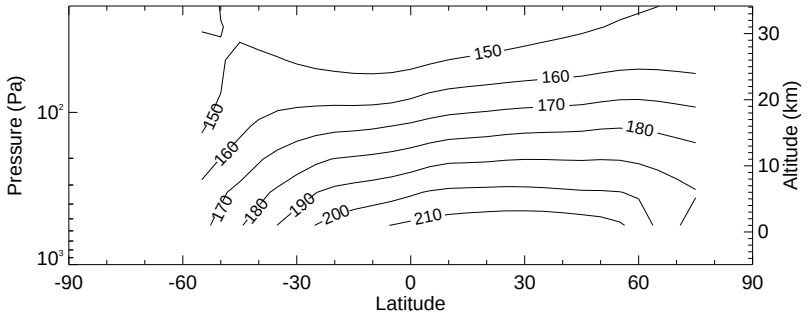

Figure 9b. Zonally averaged temperature (K) from the MCD low-dust scenario for the same period as the data in Figure 9a.

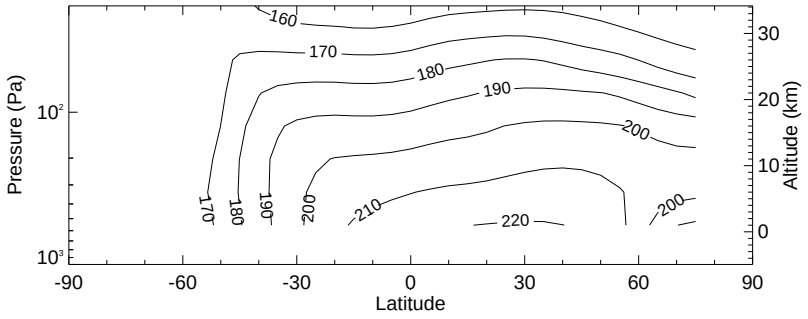

Figure 9c. Zonally averaged temperature (K) from the MCD Viking dust scenario for the same period as the data in Figure 9a.

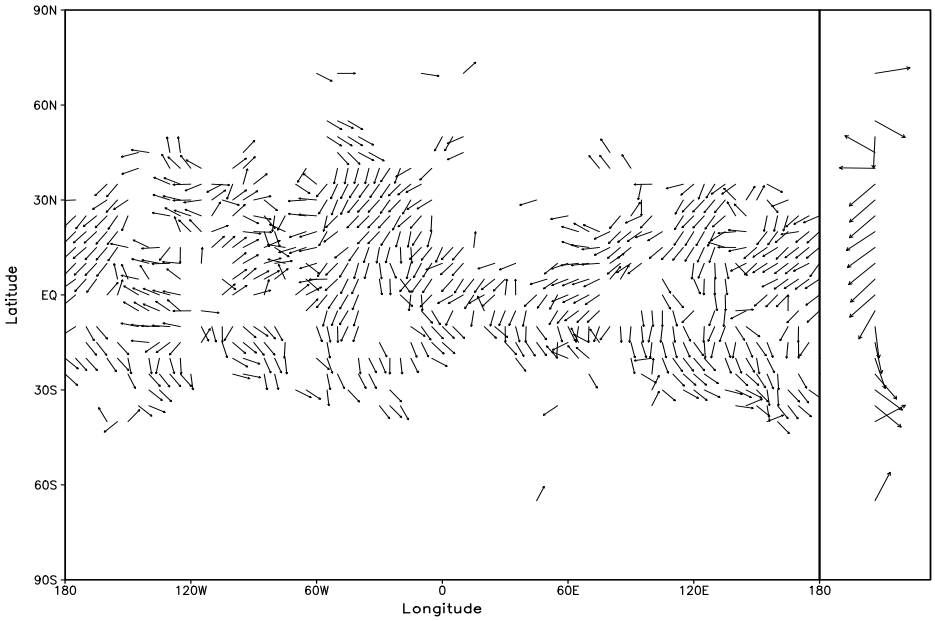

Figure 10a. Distribution of "Type I(b)" surface streak orientations derived from Viking Orbiter mosaics. The Type I(b) streaks are thought to indicate the directions of near-surface winds during the decay of the global dust storms in 1977. Average azimuths are shown for $5° \times 5°$ bins. The right panel shows the zonal average of the binned streak directions; note that there are relatively few observations more than about 30° latitude from the equator. (Average direction data from J.A. Magalhães (1998) [*Magalhães*, 1987], using data from *Thomas et al.* [1984].)

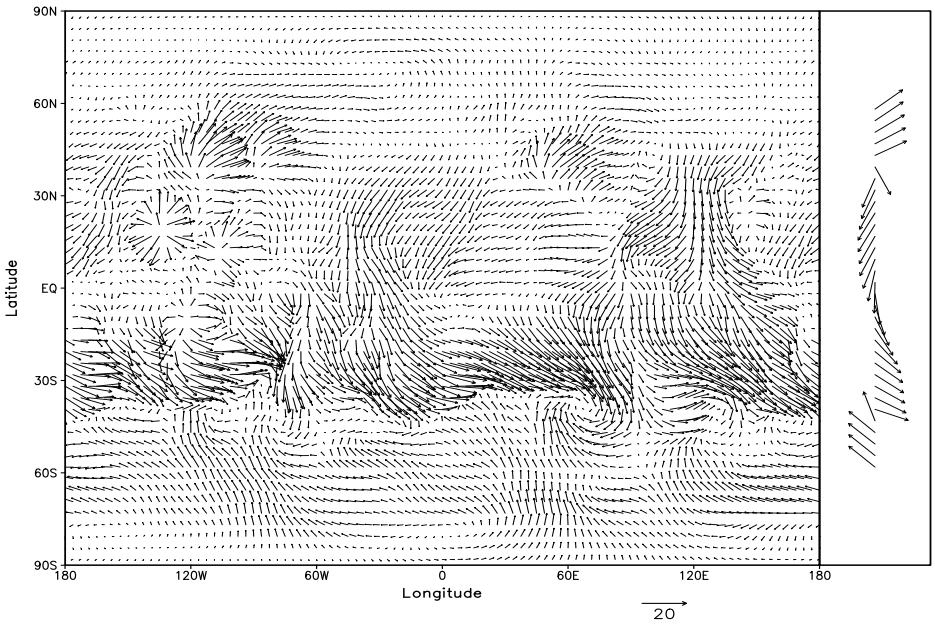

Figure 10b. Winds taken from the lowest level of the MCD (approximately 5 m above the surface) and diurnally averaged over season 10 ($L_s = 270°$–$300°$) of the $\tau = 2$ dust storm scenario; the length of a vector representing a wind of 20 m/s is indicated. The right panel shows the zonal-mean wind direction between 60°S and 60°N, to be compared with Figure 10a.

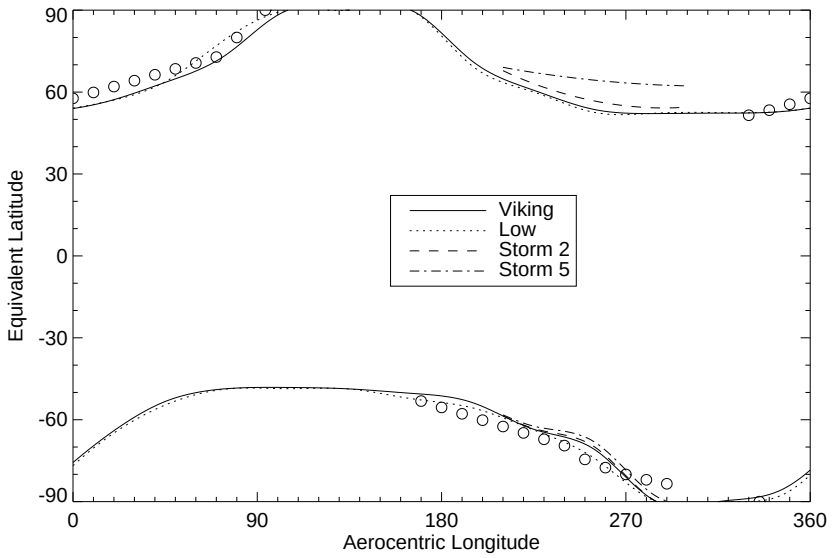

Figure 11. Mean equivalent latitudes for the edges of the polar caps of carbon dioxide ice for the four scenarios from the MCD, labeled according to the usual convention. The circles indicate observations of the equatorward boundaries of the Martian caps (data from *Pollack et al.* [1993]).

sublimation, are well predicted by the MCD models. There is perhaps some evidence of a small overestimation of the extent of the caps in the MCD. Two effects may partly contribute to this. The procedure for determining the effective size of the caps in the MCD involved adding the areas of all grid boxes in which any ice was present at all, tending to result in an overestimate if boxes were only partially icy. It is also not clear what thickness of ice cover is required to be present before the presence of a polar cap is detected in the observations.

5.5. Prediction of Mars Pathfinder Observations

The Atmospheric Structure Investigation/Meteorology experiment [*Schofield et al.*, 1997] on the Mars Pathfinder spacecraft provided the first independent test of the MCD, since the database was compiled from simulations carried out before observations from the mission became available. These new observations are compared with the MCD in this section.

The temperature profile (at 19°N, 33°W, $L_S = 142°$, 0258 LT) retrieved from Mars Pathfinder entry data [*Magalhães et al.*, 1999] was compared with the MCD (season 5, $L_S = 120°$–$150°$, 0347 LT composite mean), shown in Figure 12. As with the Viking Lander entry profiles (Figures 8a and 8b), the observations fall somewhat closer to the Viking dust climatology ($\tau \approx 0.5$ during this season). If the MCD profile is compared to the Viking Lander 1 MCD profile (Figure 8a), it can be seen that the variability model predicts a larger degree of small-scale variability in the upper atmosphere at the Pathfinder site, reflecting enhanced wave activity because of higher near-surface wind speeds. The very low temperatures seen near 80 km altitude in the observed profile are not reproduced by the mean climatology and may be reached only by addition of small-scale variability perturbations, as in Figure 12; in the observed profile these may be the result of thermal tidal components [*Magalhães et al.*, 1999]. The thermal inversion observed near 15 km altitude is presumed to be due to the presence of an ice cloud [*Schofield et al.*, 1997], which is not represented in the GCMs. The MCD does show a large thermal inversion above the surface since it is a nighttime profile; compare with Figure 8a, which is an afternoon profile at a similar latitude.

Mars Pathfinder observations of surface pressure, temperature, and wind direction over the primary 30 day phase of the mission [*Schofield et al.*, 1997] allow the MCD representation of the diurnal cycle to be tested in some detail. Both the observations and the MCD indicate very little nondiurnal variability, other than the seasonal trend, at the Pathfinder site at the time of year at which the mission landed ($L_S = 142°$); however, the diurnal cycle is strong.

The seasonal mean surface pressure cycle is compared

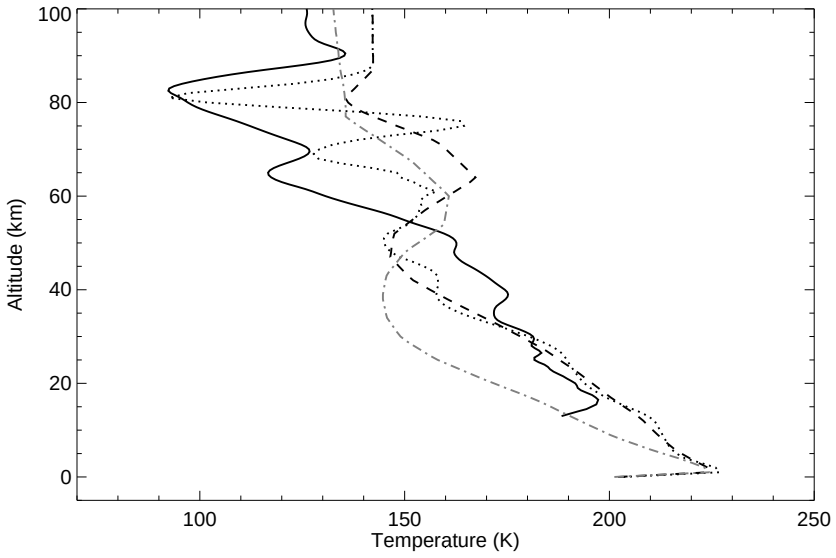

Figure 12. The Mars Pathfinder entry temperature profile (solid line), shown with MCD climatologies and variability, labeled as in Figure 8a. (Pathfinder data from J.A. Magalhães (1998) [*Magalhães et al.*, 1999].)

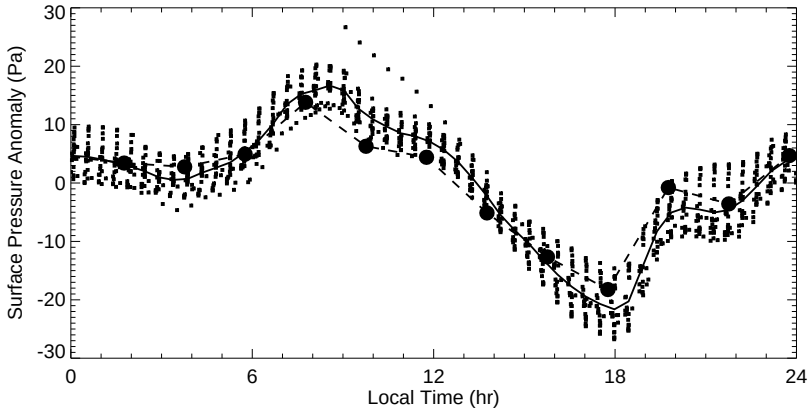

Figure 13. A comparison of the Mars Pathfinder surface pressure diurnal cycle with the MCD. The small dots show the Mars Pathfinder pressure measurements, taken 51 times per day, and the solid line is the mean of the observations taken over the first 30 days of the mission. The large circles connected by dashed lines show the MCD mean surface pressure at the Mars Pathfinder location. In both cases the diurnal-mean surface pressure has been subtracted: 666 Pa in the case of the Pathfinder data and 673 Pa in the case of the MCD.

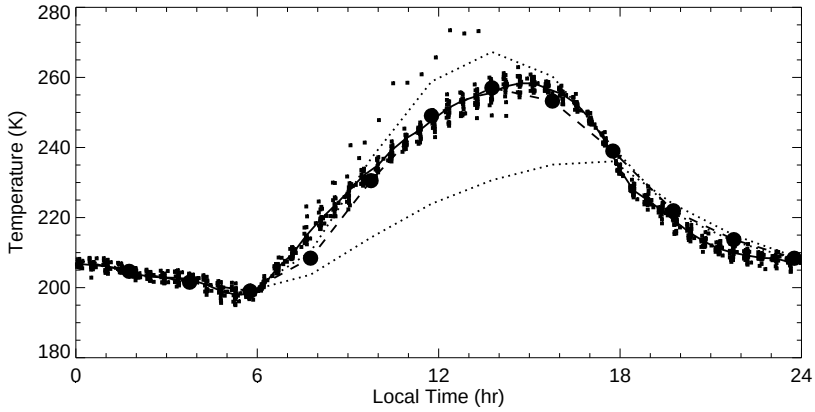

Figure 14. A comparison of the Mars Pathfinder temperature at the top of the 1 m meteorological mast with the MCD. As in Figure 13, the small dots show the individual measurements, and the solid line is the mean over 30 days. The dotted lines are the MCD surface temperature (top line at midday) and the MCD lowest atmospheric level temperature (bottom line) which is at a height of about 5 m. The large circles connected by dashed lines show a linear interpolate between the two at a height of about 1.4 m, corresponding to the top of the Pathfinder mast for comparison.

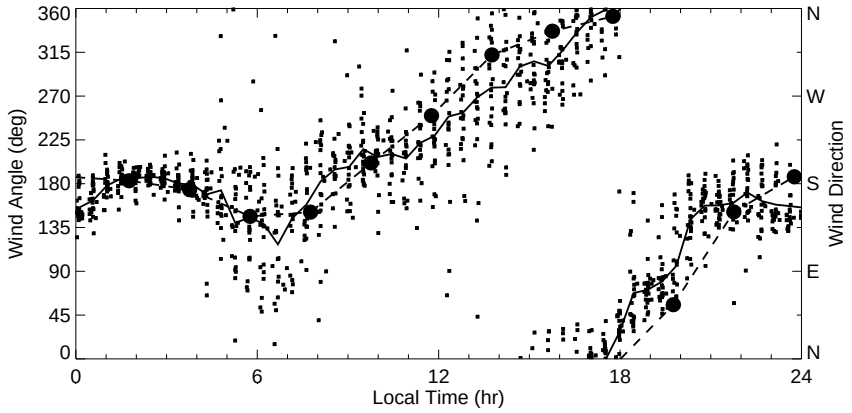

Figure 15. A comparison of the Mars Pathfinder wind direction with that at the lowest atmospheric layer in the MCD. As in Figure 13, the small dots show the individual measurements, and the solid line is the mean over 30 days. The large circles connected by dashed lines show the mean wind direction from the same point in the MCD. The wind direction axis indicates the compass point which the wind is blowing from; a wind angle of 0° is a northerly. The general sense of rotation is determined by the passage of the diurnal thermal tide; the details, such as the small rotation toward an easterly near dawn before the subsequent rotation to a westerly, are a consequence of the details of the topography.

Table 4. Surface Pressure Tides

	Amplitude, Pa		Phase, hours[a]	
Period	MPF	MCD	MPF	MCD
Diurnal	11.9	10.7	6.6	6.1
Semidiurnal	6.9	6.1	10.4	9.7

Mars Pathfinder observations are labeled MPF; database results are labeled MCD.
[a]Local time of first maximum.

with Pathfinder data in Figure 13 and can be seen to be in excellent agreement with the observations. The amplitudes and phases of the diurnal and semidiurnal tides were also calculated both from the observations and from the MCD and show reasonable agreement in both cases; see Table 4. Figure 14 shows the temperature on the Pathfinder meteorological mast compared with MCD predictions, and Figure 15 shows the wind direction; unfortunately, the wind amplitude is not well calibrated in the observations at this stage and cannot be compared. In each case the MCD prediction is remarkably good, especially considering the spatial resolution of the database and the comparison with a single point observation. It is therefore possible to have confidence in the representation of the diurnal cycle in the MCD, at least in as far as it is possible to test it at this stage.

6. Conclusions

A Mars Climate Database for use both as an engineering resource and as a scientific database has been compiled from the results of GCM experiments, rather than directly from empirical fits to observational data. The Mars GCM parameters used to compile the MCD have been taken where possible to be consistent with independent estimates of these parameters and to obtain model results which are consistent with most of the the available observational data for the atmosphere of Mars, obtained primarily by the Mariner 9 and Viking spacecraft. However, such observations are sparse in both spatial and temporal coverage. One particular strength of using a GCM to compile such a database is that it provides a physically consistent estimate of the environmental conditions on Mars for seasons and dust loadings which are not covered by the observations. The MCD has been validated against observations where appropriate, including the latest ones from the Mars Pathfinder mission.

The overall structure and organization of the database are well suited not only for extracting realistic simulated data for engineering studies of spacecraft descent trajectories or aerobraking scenarios, but also for summarizing and presenting the complex evolution of the Martian meteorology contained in the full GCM simulation during the annual seasonal and diurnal cycles for scientific purposes. All climate modelers, whether for the Earth or for other systems such as Mars, are faced with the formidable task of summarizing the results of their model simulations and usually resort to the compilation of spatially and temporally averaged statistics to reduce the data budget to a manageable level. The result is often in the form of a "climate atlas" comprising maps and tables of the distribution of various averaged variables [e.g., *Hoskins et al.*, 1989]. In the present organization of our database we have developed a strategy which enables the retention of scientifically useful information from the original high-resolution model simulations on both diurnal and seasonal timescales while keeping the data budget within 1 Gb or so. We would therefore commend the structure outlined above to other groups and agencies with an interest in summarizing large data sets, either from models or from observational analyses. The use of such an organizational standard would greatly facilitate comparisons between results obtained using different models and between models and observations to extend the verification of existing and future models.

In future versions of the GCMs the physical parameterization schemes will be enhanced and extended. Two major enhancements will involve inclusion of a dust transport model and the extension of the model top upward toward the base of the thermosphere. The lifting, transport, and deposition of dust will be modeled explicitly to alleviate the problem of having to specify the dust distribution arbitrarily; this may involve the storage of additional dust scenarios within future versions of the MCD. The altitude of the model top will be increased to at least 120 km to make the MCD more useful for aerobraking studies. This will require a substantially enhanced radiative transfer parameterization. The model-dependent nature of the upper atmosphere circulation, described by *Forget et al.* [this issue], means that at present a full data set is maintained from the results of both the Laboratoire de Météorologie Dynamique and Oxford models, although over most of the atmosphere the model differences are much smaller than the intrinsic model variability and negligible compared to the differences between different dust scenarios. It therefore makes little difference for many purposes which data set is used, though having access to both is valuable for assessing the confidence which may be placed in predictions. It is hoped that upward extensions to the model domain and further intercomparison studies will enable the upper atmosphere model dependency to be reduced and perhaps allow a single, amalgamated data

set to be presented if required.

The representation of variability within the MCD currently models only correlation of variables in the vertical. The next version to be released will include a large-scale variability model based on two-dimensional, multivariate EOFs which can describe the longitudinal propagation of baroclinic waves and allow a greater fraction of the variability to be represented with realistic horizontal, as well as vertical, correlations.

In addition to technical improvements in the model and database, the model parameters and physical schemes will be updated with the advent of new spacecraft data from missions such as Mars Global Surveyor and the recently launched Mars Climate Orbiter. With the analysis of these data the Mars GCMs will be improved and the MCD will be further updated for future engineering and scientific studies.

Appendix: Access to the Mars Climate Database

The MCD is available for distribution on various media, requiring about 1 Gb for a full installation of the scenarios from one GCM, which is recommended for serious use. The data are distributed in portable binary formats, such as the Data Retrieval and Storage (DRS) library developed for the Program for (Terrestrial) Climate Model Diagnosis and Intercomparison [e.g., *Gates*, 1992], to facilitate the transfer of data between different platforms. Bearing in mind the potentially diverse range of users of the MCD, including engineers involved in the design of spacecraft missions, scientists specializing in GCM studies who are familiar with manipulating similar data sets and scientists from other areas who may require information on environmental conditions on Mars, the data may be accessed by several methods. An interface is provided, which appears to the user to be similar to MarsGRAM [*Justus et al.*, 1996a]. Alternatively, a library of subroutines for extraction and manipulation of data which can be called by user-written programs is supplied with the MCD. As the database is written in a standard format, there is a range of meteorological graphical packages which can be utilized to access and plot data directly. Finally, access to the MCD data in a variety of graphical and numerical formats is also possible through a WWW interface: http://www.lmd.jussieu.fr/mars.html.

Acknowledgments. We are grateful for the support for this work from the European Space Agency under ESTEC contract 11369/95/NL/JG(SC) and from the UK Particle Physics and Astronomy Research Council (Oxford) and CNRS (LMD) during the development of the models.

References

Anderson, E., and C. Leovy, Mariner 9 television limb observations of dust and ice hazes on Mars, *J. Atmos. Sci.*, *35*, 723–734, 1978.

Barnes, J. R., Time spectral analysis of mid-latitude disturbances in the Martian atmosphere, *J. Atmos. Sci.*, *37*, 2002–2015, 1980.

Barnes, J. R., Midlatitude disturbances in the Martian atmosphere: A second Mars year, *J. Atmos. Sci.*, *38*, 225–234, 1981.

Chassefiere, E., P. Drossart, and O. Korablev, Post-Phobos model for the altitude and size distribution of dust in the low Martian atmosphere, *J. Geophys. Res.*, *100*, 5525–5539, 1995.

Christensen, E. J., Martian topography derived from occultation, radar, spectral and optical measurements, *J. Geophys. Res.*, *80*, 2909–2913, 1975.

Clancy, R. T., and S. W. Lee, A new look at dust and clouds in the Mars atmosphere: Analysis of emission-phase-function sequences from global Viking IRTM observations, *Icarus*, *93*, 135–158, 1991.

Clancy, R. T., A. W. Grossman, M. J. Wolff, P. B. James, D. J. Rudy, Y. N. Billawala, B. J. Sandor, S. W. Lee, and D. O. Muhleman, Water vapor saturation at low altitudes around Mars aphelion: A key to Mars climate?, *Icarus*, *122*, 32–62, 1996.

Collins, M., S. R. Lewis, P. L. Read, and F. Hourdin, Baroclinic wave transitions in the Martian atmosphere, *Icarus*, *120*, 344–357, 1996a.

Collins, M., S. R. Lewis, P. L. Read, N. P. J. Thomas, O. Talagrand, F. Forget, R. Fournier, F. Hourdin, and J.-P. Huot, A climate database for the Martian atmosphere, in *Environment Modelling for Space-Based Applications, Eur. Space Agency Spec. Publ., ESA SP–392*, 323–327, 1996b.

Collins, M., S. R. Lewis, and P. L. Read, Gravity wave drag in a global circulation model of the Martian atmosphere: Parameterisation and validation, *Adv. Space Res., 19(8)*, 1245–1254, 1997.

Forget, F., F. Hourdin, and O. Talagrand, CO_2 snow fall on Mars: Simulation with a general circulation model, *Icarus, 131*, 302–316, 1998.

Forget, F., F. Hourdin, R. Fournier, C. Hourdin, O. Talagrand, M. Collins, S. R. Lewis, P. L. Read, and J.-P. Huot, Improved general circulation models of the Martian atmosphere from the surface to above 80 km, *J. Geophys. Res., 104*, 24,155–24,176, 1999.

Gates, W. L., AMIP the atmospheric model intercomparison project, *Bull. Am. Meteorol. Soc., 73*, 1962–1970, 1992.

Greeley, R., A. Skypeck, and J. B. Pollack, Martian aeolian features and deposits: Comparisons with general circulation model results, *J. Geophys. Res., 98*, 3093–3123, 1993.

Haberle, R. M., J. B. Pollack, J. R. Barnes, R. W. Zurek, C. B. Leovy, J. R. Murphy, H. Lee, and J. Schaeffer, Mars atmospheric dynamics as simulated by the NASA/Ames general circulation model, 1, The zonal-mean circulation, *J. Geophys. Res., 98*, 3093–3123, 1993.

Hoskins, B. J., H. H. Hsu, I. N. James, M. Masutani, P. D. Sardeshmukh, and G. H. White, Diagnostics of the global atmospheric circulation, based on ECMWF analyses 1979–1989, *Tech. Rep. WMO/TD No. 326*, World Meteorol. Organ., Geneva, 1989.

Hourdin, F., P. Le Van, F. Forget, and O. Talagrand, Meteorological variability and the annual surface pressure cycle on Mars, *J. Atmos. Sci., 50*, 3625–3640, 1993.

Hourdin, F., F. Forget, and O. Talagrand, The sensitivity of the Martian surface pressure to various parameters: A comparison between numerical simulations and Viking observations, *J. Geophys. Res.*, *100*, 5501–5523, 1995.

Jaquin, F., P. Gierasch, and R. Kahn, The vertical structure of limb hazes in the Martian atmosphere, *Icarus*, *68*, 442–461, 1986.

Joshi, M. M., S. R. Lewis, P. L. Read, and D. C. Catling, Western boundary currents in the Martian atmosphere: Numerical simulations and observational evidence, *J. Geophys. Res.*, *100*, 5485–5500, 1995.

Justus, C. G., B. F. James, and D. L. Johnson, Mars Global Reference Atmospheric Model (Mars-GRAM 3.34): Programmer's guide, *Tech. Rep. NASA TM-108509*, NASA, Washington, DC, 1996a.

Justus, C. G., D. L. Johnson, and B. F. James, A revised thermosphere for the Mars Global Reference Atmospheric Model (Mars-GRAM version 3.4), *Tech. Rep. NASA TM-108513*, NASA, Washington, DC, 1996b.

Leovy, C. B., Martian meteorological variability, *Adv. Space Res.*, *2(2)*, 19–44, 1982.

Lindal, G. F., H. B. Hotz, D. N. Sweetnam, Z. Shippony, J. P. Brenkle, G. V. Hartsel, R. T. Spear, and W. H. Michael, Viking radio occultation measurements of the atmosphere and topography on Mars, *J. Geophys. Res.*, *84*, 8443–8456, 1979.

Lopez-Valverde, M. A., and M. Lopez-Puertas, A non-local thermodynamic equilibrium radiative transfer model for infrared emissions in the atmosphere of Mars, 1, Theoretical basis and nighttime populations of vibrational states, *J. Geophys. Res.*, *99*, 13,093–13,115, 1994.

Magalhães, J. A., The Martian Hadley circulation: Comparison of "viscous" model predictions to observations, *Icarus*, *70*, 442–468, 1987.

Magalhães, J. A., J. T. Schofield, and A. Seiff, Results of the Mars Pathfinder atmospheric structure investigation, *J. Geophys. Res.*, *104*, 8943–8956, 1999.

Martin, T. Z., and M. I. Richardson, New dust opacity mapping from Viking infrared thermal mapping data, *J. Geophys. Res.*, *98*, 10,941–10,949, 1993.

Mo, K. C., and M. Ghil, Statistics and dynamics of persistent anomalies, *J. Atmos. Sci.*, *55*, 877–901, 1987.

NASA, Mission to Mars: Digital Topographic Map, version 2, *USA–NASA–PDS–VO–2007*, NASA, Washington, DC, 1993.

North, G. R., Empirical orthogonal functions and normal modes, *J. Atmos. Sci.*, *41*, 879–887, 1984.

Palmer, T. N., G. J. Shutts, and R. Swinbank, Alleviation of a systematic westerly bias in general circulation and numerical weather prediction models through an orographic gravity wave drag parametrisation, *Q. J. R. Meteorol. Soc.*, *112*, 1001–1039, 1986.

Pollack, J. B., R. M. Haberle, J. R. Murphy, and H. Schaeffer, J.and Lee, Simulations of the general circulation of the Martian atmosphere, 2, Seasonal pressure variations, *J. Geophys. Res.*, *98*, 3149–3181, 1993.

Schofield, J. T., D. Crisp, J. R. Barnes, R. M. Haberle, J. A. Magalhães, J. R. Murphy, A. Seiff, S. Larsen, and G. Wilson, The Mars Pathfinder Atmospheric Structure Investigation/ Meteorology (ASI/MET) experiment, *Science*, *278*, 1752–1757, 1997.

Seiff, A., and D. B. Kirk, Structure of the atmosphere of Mars in summer at mid-latitudes, *J. Geophys. Res.*, *82*, 4364–4378, 1977.

Smith, D. E., et al., Topography of the northern hemisphere of Mars from the Mars Orbiter Laser Altimeter, *Science*, *279*, 1686–1692, 1998.

Thomas, P. C., J. Veverka, D. Gineris, and L. Wong, "Dust" streaks on Mars, *Icarus*, *49*, 398–415, 1984.

Wilson, R. J., and K. Hamilton, Comprehensive model simulation of thermal tides in the Martian atmosphere, *J. Atmos. Sci.*, *53*, 1290–1326, 1996.

Wilson, R. J., and M. I. Richardson, The Martian atmosphere during the Viking mission, 1, infrared measurements of atmospheric temperatures revisited, *Icarus*, p. in press, 1999.

Wu, S. S. C., Mars synthetic topographic mapping, *Icarus*, *33*, 417–440, 1978.

Zurek, R. W., and L. J. Martin, Interannual variability of planet-encircling dust storms on Mars, *J. Geophys. Res.*, *98*, 3247–3259, 1993.

Zurek, R. W., J. R. Barnes, R. M. Haberle, J. B. Pollack, J. E. Tillman, and C. B. Leovy, Dynamics of the atmosphere of Mars, in *Mars*, edited by H. H. Kieffer et al., pp. 835–933, Univ. of Ariz. Press, Tucson, 1992.

M. Collins, Hadley Centre for Climate Prediction and Research, U.K. Meteorological Office, London Road, Bracknell RG12 2SZ, England. (matcollins@meto.gov.uk)

F. Forget, C. Hourdin, F. Hourdin and O. Talagrand, Laboratoire de Météorologie Dynamique du Centre National de la Recherche Scientifique, Université Paris 6, 4 place Jussieu, 75252 Paris Cedex 05, France. (forget@lmd.jussieu.fr; chourdin@lmd.jussieu.fr; hourdin@lmd.jussieu.fr; talagran@lmd.ens.fr)

R. Fournier, Laboratoire d'Energie Solaire et Thermique de l'Habitat, Université Paul Sabatier, Toulouse, France. (rfo@sphinx.ups-tlse.fr)

J.-P. Huot, Space Systems Environment and Effects Analysis Section, European Space Research and Technology Centre, European Space Agency, Keplerlaan 1, 2200 AG Noordwijk, Netherlands. (jhuot@estec.esa.nl)

S. R. Lewis and P. L. Read, Atmospheric, Oceanic and Planetary Physics, Clarendon Laboratory, Parks Road, Oxford OX1 3PU, England. (s.lewis1@physics.oxford.ac.uk; p.read1@physics.oxford.ac.uk)

Received January 21, 1999; revised May 6, 1999; accepted May 14, 1999.